



AMERICAN METEOROLOGICAL SOCIETY

Journal of Atmospheric and Oceanic Technology

EARLY ONLINE RELEASE

This is a preliminary PDF of the author-produced manuscript that has been peer-reviewed and accepted for publication. Since it is being posted so soon after acceptance, it has not yet been copyedited, formatted, or processed by AMS Publications. This preliminary version of the manuscript may be downloaded, distributed, and cited, but please be aware that there will be visual differences and possibly some content differences between this version and the final published version.

The DOI for this manuscript is doi: 10.1175/JTECH-D-16-0148.1

The final published version of this manuscript will replace the preliminary version at the above DOI once it is available.

If you would like to cite this EOR in a separate work, please use the following full citation:

Guerra Paris, M., and J. Thomson, 2017: TURBULENCE MEASUREMENTS FROM 5-BEAM ACOUSTIC DOPPLER CURRENT PROFILERS. *J. Atmos. Oceanic Technol.* doi:10.1175/JTECH-D-16-0148.1, in press.



TURBULENCE MEASUREMENTS FROM 5-BEAM ACOUSTIC DOPPLER CURRENT PROFILERS

Maricarmen Guerra* and Jim Thomson

Applied Physics Laboratory, University of Washington, Seattle, Washington

*Corresponding author address: Maricarmen Guerra, Applied Physics Laboratory, University of Washington, 1013 NE 40th Street, Box 355640, Seattle, WA 98105-6698.

E-mail: mguerrap@uw.edu

ABSTRACT

Two new 5-beam Acoustic Doppler Current Profilers, the Nortek Signature 1000 AD2CP and the Teledyne RDI Sentinel V50, are demonstrated to measure turbulence at two energetic tidal channels within Puget Sound, WA, USA. The quality of the raw data is tested by analyzing the turbulent kinetic energy frequency spectra, the turbulence spatial structure function, the shear in the profiles, and the covariance Reynolds stresses. The 5-beam configuration allows for a direct estimation of the Reynolds stresses from along-beam velocity fluctuations. The Nortek's low Doppler noise and high sampling frequency allow for the observation of the turbulent inertial subrange in both the frequency spectra and in the turbulence structure function. The turbulence parameters obtained from the 5-beam Acoustic Doppler Current Profilers are validated with turbulence data from simultaneous measurements with Acoustic Doppler Velocimeters. These combined results are then used to assess a turbulent kinetic energy budget, in which depth profiles of the turbulent kinetic energy dissipation and production rates are compared. The associated codes are publicly available on the Matlab File Exchange website.

24 **1. Introduction**

25 Acoustic Doppler Current Profilers (ADCPs) are commonly used to measure the horizontal com-
26 ponents of fluid velocities along depth profiles in the ocean using three or four diverging acoustic
27 beams. The raw data from ADCPs, termed pings, correspond to single velocity measurements in
28 the along-beam direction. The raw ping data are typically burst-averaged in time (5 -10 minutes
29 for tidal flows to ensure stationary mean flow conditions (McCaffrey et al. 2015)). Averaging re-
30 duces the Doppler noise inherent to the measurement, which can add significant variance to the
31 raw signals (above and beyond the variance due to real turbulent fluctuations) (Brumley et al.
32 1991). However, if the raw along-beam velocities are retained, many turbulence parameters, such
33 as turbulent kinetic energy dissipation rates and Reynolds stresses, can be estimated from ADCP
34 measurements. Estimation methods are based on the variance and correlations of the along-beam
35 velocity fluctuations, often with explicit removal of the variance contributed by the Doppler noise
36 (Lu and Lueck 1999; Stacey et al. 1999; Wiles et al. 2006; Thomson et al. 2012).

37 Indirect methods to estimate turbulent dissipation rates, such as turbulence kinetic energy (TKE)
38 spectra and the turbulence structure functions (Pope 2001), are based on Kolmogorov's hypothesis
39 about the existence of a range of turbulent length scales within the isotropic turbulence energy
40 cascade, known as inertial subrange, in which the energy transfer is solely determined by the
41 dissipation rate (Kolmogorov 1941; Pope 2001). The application of these methods requires the
42 observation the inertial subrange in the data (Pope 2001).

43 In the frequency domain, some authors (e.g Thomson et al. 2012; Richard et al. 2013; Durgesh
44 et al. 2014) have attempted to use spectra calculated from raw along-beam velocity ADCP data,
45 but the inherent Doppler noise typically obscures the inertial subrange (Richard et al. 2013). Re-
46 cently, turbulence dissipation rates have been estimated from turbulence spectra after averaging

47 the frequency spectra for different mean flows and bins in order to successfully observe the iner-
48 tial subrange in the turbulence energy cascade in McMillan et al. (2016) and McMillan and Hay
49 (2017). Another common technique is to estimate turbulent dissipation rates using the second-
50 order spatial structure function of turbulence (Wiles et al. 2006; Rusello and Cowen 2011).

51 One of the most frequently used techniques to estimate Reynolds stresses from ADCP along-
52 beam velocities is the variance technique (Lu and Lueck 1999; Stacey et al. 1999; Rippeth et al.
53 2003), which provides two components (out of six) of the Reynolds stresses and is based on the
54 variance of opposite beam velocity fluctuations.

55 A new generation of broadband 5-beam ADCPs with the ability to measure flow velocity at
56 higher frequencies and with lower noise levels is poised to expand routine turbulence measure-
57 ments. Moreover, the inclusion of a fifth beam allows for a true measurement of vertical velocities
58 and the estimation of five (out of six) Reynolds stresses, total turbulent kinetic energy (TKE),
59 and anisotropy directly from the along-beam velocities (Lu and Lueck 1999; Dewey and Stringer
60 2007). This is a notable expansion beyond the four-beam variance methods (Lu and Lueck 1999;
61 Stacey et al. 1999; Rippeth et al. 2003). These new features, together with the integration of iner-
62 tial motion units, might even expand the application of these ADCPs to the study of upper ocean
63 turbulence and wave breaking turbulence, and to improve the estimation of parameters used in
64 turbulence models.

65 This paper presents turbulence measurements from two new 5-beam acoustic current profil-
66 ers: the Nortek Signature 1000 (kHz), which uses the acronym AD2CP to distinguish it from the
67 previous generation of profilers, and the new Teledyne RDI Sentinel V50 500 (kHz). The new
68 instruments' capabilities are assessed in two field deployments in highly energetic tidal channels,
69 calculations of turbulence parameters, and the subsequent evaluation of turbulent kinetic energy
70 (TKE) budgets.

71 The results are validated using measurements from Acoustic Doppler Velocimeters (ADV),
72 which are typically the preferred choice for turbulence measurements. However, ADVs only mea-
73 sure at a point, and their deployment at mid-depths requires complicated moorings and subsequent
74 motion corrections to the raw data (Thomson et al. 2013). The new ADCPs are shown to be a
75 more practical alternative to ADVs, with the potential for new insights about where turbulence is
76 being produced and dissipated in the water column.

77 In Section 2 details of the field measurements are presented. In Section 3, estimates of the
78 TKE dissipation rate are presented using two different methods: the TKE frequency spectra and
79 the second-order spatial structure function. In Section 4, the terms of the TKE production rate
80 are estimated; in particular, Reynolds stresses are calculated using along-beam velocities from all
81 five beams. Finally, in Section 5, the TKE dissipation and production rate estimates are used to
82 examine the TKE budget at the two tidal channels.

83 **2. Data Collection**

84 *a. Site Description*

85 Turbulence measurements were taken at Admiralty Inlet and Rich Passage, two tidal channels
86 located in Puget Sound, WA, USA. Figure 1a shows the location of the field sites and the detailed
87 locations of the instruments. A summary of the deployments and instrument settings is presented
88 in Table 1.

89 Admiralty Inlet is located in the northern part of Puget Sound (48.14°N , 122.71°W). Admiralty
90 Inlet is ~ 6.5 km wide and ~ 50 m deep at the measurement site. The principal direction of the
91 flow is $\sim 50^{\circ}$ from the east in the clockwise direction.

Rich Passage is located south of Bainbridge island in Puget Sound (47.59° N, 122.56° W). At the measurements site the channel is ~ 24 m deep and ~ 550 m wide. The channel is oriented $\sim 45^{\circ}$ from north in the clockwise direction.

b. Instruments and Settings

The 5-beam Doppler profilers were deployed mounted looking upward on separate Ocean-science Sea Spider tripods, which place each instrument ~ 0.9 m above the seafloor when deployed. The instruments have four beams slanted at 25° from the vertical, plus a fifth vertical beam. Deployments were on May 11 2015 at Admiralty Inlet and on May 17 – 18 2015 at Rich Passage. Table 1 summarizes the deployments and sampling parameters.

The Nortek Signature was configured to measure turbulence in along-beam coordinates using its five beams at 8 Hz (the maximum possible when using all five beams) for bursts lasting 10 minutes in duration. At Admiralty Inlet, the interval between bursts was 20 minutes and there were 20 velocity bins at 1 m spacing. At Rich Passage, the interval between bursts was thirty minutes and there were 15 velocity bins at 1 m spacing.

The Teledyne RDI Sentinel V50 was configured to measure along-beam turbulent velocities at 2 Hz (the maximum possible when using all five beams) for 10 minute bursts with a 20 minute interval. At Admiralty Inlet, the RDI Sentinel V50 tripod was ~ 80 m away from the Nortek Signature tripod and there were 20 velocity bins at 1 m spacing. At Rich Passage, the Sentinel V50 was not deployed (it was unavailable).

In addition to the two 5-beam Acoustic Doppler Current Profilers, Acoustic Doppler Velocimeters (ADV) were deployed at both sites in the vicinity of the instruments in order to compare and validate the data from the profilers.

114 At Admiralty Inlet, a Nortek Vector ADV was deployed 130 m east of the Nortek Signature
115 on board a Tidal Turbulence Mooring (TTM) (Thomson et al. 2013; Harding et al. In revision;
116 Kilcher et al. In revision) on May 11 – 13 2015. The TTM consists of an anchor (approx. 1000
117 kg wet weight) to hold the mooring in place, a sphere (approx. 300 kg positive buoyancy) to hold
118 the mooring vertical, and an instrumentation vane inline between the anchor and the buoy where
119 the ADV was mounted. The TTM positions the ADV at 10 m above the sea bottom. The ADV
120 was set to measure velocities at 16 Hz continuously. An inertial motion unit (IMU) synchronously
121 measured TTM acceleration and orientation; these data are used to remove contaminations of
122 mooring motion from the ADV turbulent velocities. The motion correction method is described in
123 detail in Thomson et al. (2013) and Kilcher et al. (In revision).

124 At Rich Passage, a Nortek Vector ADV was deployed in the same location as the Nortek Signa-
125 ture. The ADV was mounted on a Turbulence Torpedo (TT), a sounding weight that hangs from
126 a davit on the side of the ship while the ship is holding station (Thomson et al. 2013; Harding
127 et al. In revision; Kilcher et al. In revision). The Turbulence Torpedo ADV was deployed on June
128 5 2015, sampling turbulent velocities at 16 Hz for 2.5 hours during ebb tide (mean flow ranging
129 between 1.5 and 2 m/s). Motion corrections were applied to the velocity measurements following
130 the same methods used for the TTM ADV measurements (Thomson et al. 2013; Kilcher et al. In
131 revision).

132 *c. Raw Data*

133 Figure 2 shows vertical profiles, and time series, of along channel velocity (after a coordinate
134 transformation of the beam velocities) measured by the Nortek Signature for both study sites.
135 At Admiralty Inlet, it was possible to measure only a single tidal cycle due to the rapid battery
136 consumption when sampling at high frequency and not using external battery canisters. After

137 approximately 12 hours, the Nortek Signature kept sampling, but the bursts became shorter (less
138 than the 10 minutes setting). At Rich Passage, a reduced duty cycle made it possible to measure
139 two tidal cycles before the bursts became shorter. For both deployments, a single battery pack was
140 used, but additional battery packs can be externally connected to the instrument to overcome the
141 limits from rapid battery consumption. According to the Nortek Signature Deployment software,
142 for a deployment using the same settings as for the Admiralty Inlet Signature deployment, the
143 instrument life can be extended to 158 days when using a 3600 Wh Lithium external battery pack.
144 For the same deployment settings, a memory card of 64 GB capacity would last 179.5 days (and
145 thereby exceed the limitations of the external batteries).

146 A ten-minute time interval is selected for burst-averaging these data sets and for estimation
147 of statistical parameters (spectra, structure function, etc). This time interval is chosen as short
148 enough to remove any trend contamination from tidal currents in the turbulence time-series (i.e
149 short enough so that the tidal current does not change), but long enough to capture the large scale
150 turbulence (McCaffrey et al. 2015). An analysis of this time interval selection for turbulence
151 analysis in tidal channels is available in McCaffrey et al. (2015).

152 The maximum observed burst-averaged horizontal speed at Admiralty Inlet was 2.04 m/s during
153 flood which corresponds to a Reynolds number of $\mathcal{O}(10^8)$. At Rich Passage the maximum burst-
154 averaged observed horizontal speed was 1.95 m/s during ebb, which corresponds to a Reynolds
155 number of $\mathcal{O}(10^7)$. Although these are short datasets, they are sufficient to observe turbulent veloc-
156 ity fluctuations at a wide range of mean flow conditions at each site (e.g., 10 minute burst-averaged
157 horizontal speeds varied from 0 to 2 m/s). Data are quality controlled to remove measurements
158 with low beam correlations (less than 50) and low echo amplitude (less than 30 dB), as per manu-
159 facturer recommendation. This removes a very small fraction (less than 0.5%) of the raw data.

3. Analysis: Turbulent Kinetic Energy Dissipation Rate

At each depth in the ADCPs measured profiles, the TKE dissipation rate is estimated by two methodologies: from the frequency spectra (Lumley and Terray 1983) and from the spatial structure function (Wiles et al. 2006). Both methods are derived from Kolmogorov's turbulence hypotheses (Kolmogorov 1941; Pope 2001) and require the observation of the inertial subrange of isotropic turbulence.

a. Turbulent Kinetic Energy Spectra

The distribution of turbulent kinetic energy among eddies of different sizes is represented through the turbulent kinetic energy spectra. Assuming stationarity, the turbulence advected past the instruments at average speeds \bar{u} has frequency (f) spectra that are related to the wavenumber (k) spectra by $\bar{u} \propto f/k$ (i.e., Taylor's frozen field). Thus, the frequency spectra are expected to include an inertial sub-range, in which the turbulent kinetic energy follows $f^{-5/3}$ as a manifestation of the energy cascade following $k^{-5/3}$ (Kolmogorov 1941; Pope 2001).

TKE spectra are estimated using Welch's Overlapped Segment Averaging method applied to the vertical beam velocities (beam 5). For the Nortek Signature data sets, spectral estimates are calculated for every ten-minute burst using 23 50 s sub-windows with 50% overlap and a Hanning data taper, which results in an ensemble spectral density estimate with ~ 45 degrees of freedom. TKE spectra with the same degrees of freedom are also estimated for the RDI Sentinel V50 vertical beam velocities and for the Nortek Vector ADV measurements.

TKE spectra estimates for both sites for the tenth vertical bin (10.4 m from the sea bottom) are presented in Figure 3 colored by mean flow conditions. The TKE spectra estimates from the RDI Sentinel V50 measurements for the same bin are included in the Admiralty Inlet figures in grey. Averaged TKE spectra from the Nortek Vector ADV data is included for comparison as a red

183 dashed line when available; the range of TKE spectra from the TTM ADV data is included as a
184 pink area in the Admiralty Inlet plots. In this analysis, mean flows that are close to slack conditions
185 ($\bar{u} < 0.5$ m/s) have been removed as the spectra does not show the theoretical $f^{-5/3}$ slope. Spectral
186 density estimates from the Nortek Signature data are generally well sorted by mean flow velocity,
187 implying that a higher TKE is observed at higher mean flows. The exception is during the stronger
188 ebb at Rich Passage, where the instrument is in the lee of a sill.

189 The most novel result from the Nortek Signature data is the clear observation of the TKE energy
190 cascade in the spectral estimates, which is usually obscured by the Doppler noise of profiling
191 instruments. An isotropic region of tridimensional turbulence is present at mid frequencies ($0.1 <$
192 $f < 1$ Hz) which follows the classic $f^{-5/3}$ energy cascade (Kolmogorov 1941). At higher ($f >$
193 1 Hz) frequencies, the spectra become affected by the instrument inherent Doppler noise. The
194 spectral noise level of the Nortek Signature is observed around $S_w(f) = 10^{-4} \text{ m}^2\text{s}^{-2}\text{Hz}^{-1}$, while
195 the noise level of the Nortek Vector is observed around $S_w(f) = 10^{-5} \text{ m}^2\text{s}^{-2}\text{Hz}^{-1}$. The noise level
196 of the RDI Sentinel V50, by contrast, is much higher at $S_w(f) = 10^{-2} \text{ m}^2\text{s}^{-2}\text{Hz}^{-1}$, and thus the
197 inertial subrange is typically obscured in those spectra.

198 The lower spectral noise floor observed from the Nortek Signature data might be attributed to
199 its ability to sample faster. Even if the single-ping error were the same between the RDI Sentinel
200 V50 and the Nortek Signature, the noise floor observed in a spectral density will still be lower
201 when the sampling is faster, as it is redistributed along a wider frequency range. In order to fairly
202 compare the observed spectral noise floor of the two profilers, the data from the Nortek Signature
203 is sub-sampled down to 2 Hz and new spectra are estimated (but not shown). For the sub-sampled
204 case, the TKE energy cascade is still observed between $0.1 < f < 0.8$ Hz, and the noise level is
205 observed around $S_w(f) = 2 * 10^{-4} \text{ m}^2\text{s}^{-2}\text{Hz}^{-1}$. This is slightly higher than when sampling at 8
206 Hz, but not nearly as high as the spectral noise level of the RDI. The latter implies that even when

207 sampling at the same frequency, the Nortek Signature presents a lower Doppler noise. The higher
 208 noise level of the RDI Sentinel V50 data obscures the inertial subrange in these TKE spectra,
 209 preventing the following estimation of TKE dissipation rate.

210 Figure 4 shows spectral estimates at maximum ebb and flood at the two sites for all vertical
 211 bins from the Nortek Signature data. The spectral estimates are well-sorted by depth, except for
 212 the maximum ebb at Rich Passage due to the existence of a vertical sill upstream of the measure-
 213 ment location. TKE density decreases as the distance from the bottom increases, consistent with
 214 bottom-generated turbulence. In the higher bins, the observable portion of the inertial subrange
 215 becomes narrower due to the decrease in TKE density (i.e., the noise floor affects spectra at a
 216 lower frequency); for example at 20.4 m from the sea bottom the inertial subrange is observed at
 217 $0.1 < f < 0.6$ Hz.

218 The dissipation rate of TKE, ϵ , is related to the isotropic portion of the vertical TKE frequency
 219 spectrum by:

$$S_w(f) = \alpha \epsilon^{2/3} f^{-5/3} \left(\frac{\bar{u}}{2\pi} \right)^{2/3} \quad (1)$$

220 where α is a constant equal to 0.69 (Sreenivasan 1995), ϵ is the TKE dissipation rate, f is the
 221 frequency and \bar{u} is the mean along channel velocity. This applies Taylor's 'frozen field hypothe-
 222 sis', which assumes that the turbulence is in steady state as it advects past the instrument (neither
 223 developing nor decaying), such that we can transform the temporal observation into a spatial one
 224 (i.e., $f = \bar{u}k/2\pi$, where k is the spatial wavenumber).

225 Each estimated spectra is multiplied by $f^{5/3}$ to obtain a compensated spectra, which should be
 226 horizontal (flat) in the presence of an inertial subrange. The dissipation rate is estimated by solving
 227 $\overline{S_w(f) f^{5/3}} \Big|_{f_1}^{f_2} = \alpha \epsilon^{2/3} \left(\frac{\bar{u}}{2\pi} \right)^{2/3}$, where f_1 to f_2 is the frequency range with the slope closest to zero
 228 in the compensated spectra. The range of frequencies used to estimate the mean compensated
 229 spectra, $\overline{S_w(f) f^{5/3}}$, varies according to the position of the inertial subrange for different mean

flows and depths, ranging between $0.1 < f < 1$ Hz. A minimum of five frequencies are used to estimate dissipation rates from the compensated spectra.

Uncertainties in the TKE dissipation rates from spectra are calculated by propagating the uncertainty in the compensated spectra (Bassett et al. 2013), such that:

$$\sigma_{\varepsilon_s} = \frac{2\pi}{\bar{u}} \left(\frac{1}{\alpha} \right)^{3/2} \frac{3}{2} S_{w_{comp}}^{-1/2} \sigma_{S_{w_{comp}}} \quad (2)$$

where σ_{ε_s} is the uncertainty in the dissipation rate estimate, and $\sigma_{S_{w_{comp}}}$ is taken to be the variance of the compensated spectra in the range of frequencies used to estimate ε .

b. Turbulence Structure Function

The along-beam velocities can be used to estimate the second-order spatial structure function of the along-beam turbulent fluctuations, $D(z, r)$, following the methodology described in Wiles et al. (2006). The structure function is defined as:

$$D_i(z, r) = \langle (u'_i(z+r) - u'_i(z))^2 \rangle \quad (3)$$

where z is the along-beam measurement location, u'_i corresponds to each along-beam velocity fluctuation, and r is the distance between two velocity bins; the angle brackets denote a time average over the burst (ten-minute bursts for these data sets).

The structure function $D_i(z, r)$ is estimated from the bottom of the profile upwards. The distance r is set to be positive and limited by the distance to the closest boundary, which in these cases is the sea bottom. Figure 5 shows examples of the spatial structure function for the vertical beam turbulent fluctuations, $D_5(z, r)$, at $z = 10.4$ m from the sea bottom at both sites. The structure function estimates from the RDI Sentinel V50 measurements for the same bin are included in the Admiralty Inlet figures in grey. Structure functions from the Nortek Signature data are generally

well-sorted by the mean flow, except during the stronger ebb at Rich Passage, where again the sill creates a region of low turbulence. The slopes of the structure functions from the Nortek Signature agree well with the expected $r^{2/3}$ at both sites. Again, it is not possible to observe the theoretical $r^{2/3}$ slope in the structure function estimates from the RDI Sentinel V50. The structure function off-set at $r = 0$, N , is related to the instrument Doppler noise, σ_N , as $N = 2 * \sigma_N$ (Wiles et al. 2006; Thomson 2012). A higher offset N is observed in the RDI Sentinel V50 structure functions due to its higher Doppler noise, which prevents the structure function drop-off as r approaches zero, obscuring the $r^{2/3}$ slope, and thus limiting the estimation of the TKE dissipation rate. In these measurements, the 1 m bin size limits the observed turbulence length-scales, and particularly affects the observation of the inertial subrange in the turbulence structure function (McMillan and Hay 2017).

In the inertial subrange, the structure function is related to the distance r and to the dissipation rate ε by:

$$D_i(z, r) = C_v^2 \varepsilon^{2/3} r^{2/3} \quad (4)$$

where C_v^2 is a constant equal to 2.1 (Wiles et al. 2006; Thomson et al. 2012).

The structure function is multiplied by $r^{-2/3}$ to obtain a compensated structure function in the inertial subrange (Rusello and Cowen 2011). The dissipation rate is estimated by solving $\overline{D(z, r) r^{-2/3}} \Big|_{r_1}^{r_2} = C_v^2 \varepsilon^{2/3}$, where r_1 to r_2 is the range with the slope closest to zero. Estimates are not calculated for depths with less than four points in the structure function. At Admiralty Inlet, the minimum r range used in the estimates is 1 to 4 m and the maximum range is 1 to 10 m; at Rich Passage the minimum range is 1 to 4 m, and the maximum range is 1 to 7 m. Within the valid depths, the structure function is quality controlled to remove estimates with negative slope, resulting in a loss of 21% of valid structure functions at Admiralty Inlet and 28% at Rich Passage, for which no dissipation estimate is available. Although this is a rather severe amount of quality

control, it is less than that of other studies applying the structure function (McMillan et al. 2016; Thomson 2012).

Uncertainties in TKE dissipation rates from the structure function fitting are calculated by propagating the uncertainty in the compensated structure function, such that:

$$\sigma_{\epsilon_D} = \left(\frac{1}{Cv^2} \right)^{3/2} \frac{3}{2} \overline{D_{comp}}^{1/2} \sigma_{D_{comp}} \quad (5)$$

were σ_{ϵ_D} is the uncertainty in the dissipation rate estimate, and $\sigma_{D_{comp}}$ is taken to be the variance of the compensated structure function in the range of bin separations used to estimate ϵ .

Figure 6 shows averaged vertical profiles of TKE dissipation rates, separated by ebb and flood tides, with their corresponding error estimates for both sites and compares the two methods. The TKE dissipation rate estimates from the two methods are in agreement, although the estimates from the structure function do not cover the entire measured profile due to the r limitation. AD2CP TKE dissipation rate estimates are also in good agreement with estimates from ADV data, even at Rich Passage, where the TT ADV was located above the top of the profile measured by the Nortek Signature. Averaged uncertainties, expressed as percentage of the flood/ebb averaged TKE dissipation rates, present different patterns at each site. At Admiralty Inlet, uncertainties from the structure function range between 12%, closer to the bottom, to 22%, higher in the water column. At Rich Passage, uncertainties from the structure function method remain between 10 to 15% through the water column, while uncertainties from the TKE spectra method range between the 15%, closer to the bottom, and 25% higher in the water column.

4. Analysis: Turbulent Kinetic Energy Production Rate

In a well-mixed environment, the buoyancy TKE sink term can be neglected, and the TKE is primarily produced by the mean flow shear. If horizontal shear is small, the TKE production can be approximated in terms of the Reynolds stresses and the velocity vertical gradients as:

$$P = -\overline{u'_{ch} w'} \frac{\partial \overline{u_{ch}}}{\partial z} - \overline{v'_{ch} w'} \frac{\partial \overline{v_{ch}}}{\partial z} - \overline{w' w'} \frac{\partial \overline{w}}{\partial z} \quad (6)$$

where P is the production of TKE, u_{ch} , v_{ch} and w are the along channel, across channel and vertical velocities respectively, and the primes denote velocity fluctuations.

a. Vertical Shear

Along-beam velocities are transformed into orthogonal east-north-up components. The horizontal components are rotated to obtain along and across channel velocity components at each location. The vertical gradients of the along channel, across channel and vertical velocity, $\frac{\partial \overline{u_{ch}}}{\partial z}$, $\frac{\partial \overline{v_{ch}}}{\partial z}$, $\frac{\partial \overline{w}}{\partial z}$, are estimated as the centered difference of their burst-average using the vertical distance between measurements.

The uncertainty in the shear estimations is calculated following Williams and Simpson (2004) method as:

$$\sigma_S^2 = \frac{\sigma_N^2}{M \Delta z^2 \sin^2 2\theta} \quad (7)$$

where σ_N is the instrument inherent Doppler noise, M is the number of samples used in the burst-averaged and θ is the beam inclination angle. This estimate corresponds to the minimum level of shear detection considering only instrument noise as a source of error in the measurements (Williams and Simpson 2004). It has been previously reported that instrument noise from

instrument softwares is usually biased low (Williams and Simpson 2004; Thomson et al. 2012). In this study, the instrument noise is estimated from the spectral noise level, as it is considered to be white noise (i.e. has a constant horizontal spectra) (McMillan and Hay 2017). The estimated ping-to-ping instrument noise levels from spectra are: $\sigma_N = 2.65$ cm/s for the Nortek Signature, and $\sigma_N = 5.39$ cm/s for the RDI Sentinel V50. Instrument noise reported by the instruments corresponding software for each deployment and empirically estimated noise are shown in Table 1.

b. Reynolds Stresses

The Reynolds stress tensor is estimated following the methodology of Dewey and Stringer (2007) for a 5-beam ADCP configuration. This methodology extends the variance technique (Lu and Lueck 1999; Stacey et al. 1999; Rippeth et al. 2003) to different ADCP beam configurations including expressions for the Reynolds stresses for non-zero tilt. The use of five beams allows for exact expressions for five of the Reynolds stresses, total TKE and anisotropy (Dewey and Stringer 2007). This method assumes small angle approximations for pitch and roll, which were achieved in these deployments (mean pitch $\sim 2.3^\circ$ and mean roll $\sim 0.4^\circ$ at Admiralty Inlet, mean pitch $\sim 0.35^\circ$ and mean roll $\sim -1.19^\circ$ at Rich Passage). The Reynolds stresses from Dewey and Stringer (2007) are written in instrument coordinates (assuming heading is equal to zero), thus the obtained stresses are rotated to along and across channel coordinates after the calculations.

The following equations, from Dewey and Stringer (2007), define the Reynolds stresses in instruments coordinates for any 5-beam ADCP, assuming small tilt angles approximation:

$$\begin{aligned} \overline{u'^2} = \frac{-1}{4 \sin^6 \theta \cos^2 \theta} \{ & -2 \sin^4 \theta \cos^2 \theta (\overline{u_2'^2} + \overline{u_1'^2} - 2 \cos^2 \theta \overline{u_5'^2}) \\ & + 2 \sin^5 \theta \cos \theta \phi_3 (\overline{u_2'^2} - \overline{u_1'^2}) \} \end{aligned} \quad (8)$$

$$\overline{v'^2} = \frac{-1}{4 \sin^6 \theta \cos^2 \theta} \{ -2 \sin^4 \theta \cos^2 \theta (\overline{u_4'^2} + \overline{u_1'^2} - 2 \cos^2 \theta \overline{u_5'^2}) - 2 \sin^4 \theta \cos^2 \theta \phi_3 (\overline{u_2'^2} - \overline{u_1'^2}) \quad (9)$$

$$+ 2 \sin^3 \theta \cos^3 \theta \phi_3 (\overline{u_2'^2} - \overline{u_1'^2}) - 2 \sin^5 \theta \cos \theta \phi_2 (\overline{u_4'^2} - \overline{u_3'^2}) \}$$

$$\overline{w'^2} = \frac{-1}{4 \sin^6 \theta \cos^2 \theta} \{ -2 \sin^5 \theta \cos \theta \phi_3 (\overline{u_2'^2} - \overline{u_1'^2}) + 2 \sin^5 \theta \cos \theta \phi_2 (\overline{u_4'^2} - \overline{u_3'^2}) \quad (10)$$

$$- 4 \sin^6 \theta \cos^2 \theta \overline{u_5'^2} \}$$

$$\overline{u'w'} = \frac{-1}{4 \sin^6 \theta \cos^2 \theta} \{ \sin^5 \theta \cos \theta (\overline{u_2'^2} - \overline{u_1'^2}) + 2 \sin^4 \theta \cos^2 \theta \phi_2 (\overline{u_2'^2} + \overline{u_1'^2}) \quad (11)$$

$$- 4 \sin^4 \theta \cos^2 \theta \phi_3 \overline{u_5'^2} - 4 \sin^6 \theta \cos^2 \theta \phi_2 \overline{u'v'} \}$$

$$\overline{v'w'} = \frac{-1}{4 \sin^6 \theta \cos^2 \theta} \{ \sin^5 \theta \cos \theta (\overline{u_4'^2} - \overline{u_3'^2}) - 2 \sin^4 \theta \cos^2 \theta \phi_2 (\overline{u_4'^2} + \overline{u_3'^2}) \quad (12)$$

$$+ 4 \sin^4 \theta \cos^2 \theta \phi_3 \overline{u_5'^2} + 4 \sin^6 \theta \cos^2 \theta \phi_3 \overline{u'v'} \}$$

where θ is the beam inclination angle (25° in these cases), ϕ_2 and ϕ_3 correspond to Dewey's pitch and roll respectively, and $\overline{u_i'^2}$ are the along-beam velocity fluctuation variances. For the Nortek Signature configuration: ϕ_2 corresponds to negative roll, and ϕ_3 to pitch, and $u_1 = u_{1Sig}$, $u_2 = u_{3Sig}$, $u_3 = u_{4Sig}$, and $u_4 = u_{2Sig}$. For the RDI Sentinel V50: ϕ_2 corresponds to roll, and ϕ_3 to pitch, and $u_1 = u_{2Sent}$, $u_2 = u_{1Sent}$, $u_3 = u_{4Sent}$, and $u_4 = u_{3Sent}$.

The Reynolds stress tensors are quality controlled to be a positive definite matrix. A total of 12% of the Reynolds stress tensors at Admiralty Inlet, and an 8% at Rich Passage, do not meet this requirement.

The uncertainty in the Reynolds stresses estimations is calculated following Williams and Simpson (2004) method as:

$$\sigma_{RS}^2 = \frac{\sigma_N^4}{M \sin^2 2\theta} \quad (13)$$

where σ_N is the instrument noise, M is the number of samples used in the averaging and θ is the beam inclination angle. This uncertainty estimate corresponds to the minimum level of

Reynolds stress detection only considering instrument noise as for the estimation of shear uncertainty (Williams and Simpson 2004). This uncertainty will be used in the estimation of TKE Production uncertainty.

A comparison between the obtained Reynolds stresses from the 5-beam profilers (after noise removal) and from direct covariance with the TTM ADV at Admiralty Inlet are shown in the scatter plot of Figure 7. Blue and red dots are averages binned by $\overline{u'_{ch}w'}$ from the TTM ADV measurements. Despite large scatter in the comparison, the binned results are in agreement at higher Reynolds stresses. The large differences might be explained by the separation of the instruments and by remaining noise in the Reynolds stress estimates.

Figures 8 and 9 show time series of vertical profiles of the five Reynolds stresses estimated following the Dewey and Stringer (2007) method at Admiralty Inlet and Rich Passage respectively. The horizontal Reynolds stresses ($\overline{u'^2_{ch}}, \overline{v'^2_{ch}}$) reach values that are an order of magnitude higher than the rest of the estimated Reynolds stresses at both sites. The magnitude of the Reynolds stresses are modulated by the tidal currents. At Admiralty Inlet, Reynolds stresses magnitudes increase as the horizontal speed increases, and the maximum values are observed during the observed ebb. At Rich Passage (Figure 9), the Reynolds stresses magnitude also increases with the horizontal speed. The highest Reynolds stresses are observed during the highest flood tidal current.

Figure 10 shows vertical profiles of the estimated vertical shear Reynolds stress ($\overline{u'_{ch}w'}$), averaged for ebb and flood at the two sites together with ADV estimates when available. Additionally, estimates using the variance technique with no tilt corrections for the two 5-beam Acoustic Doppler Current Profilers at both sites are included.

At Admiralty Inlet, during ebb, averaged estimates from the two instruments are in good agreement, and are also in good agreement with the TTM ADV estimates. For the first 15 m of the water column, the estimates from the Nortek Signature are higher than those from the RDI Sen-

363 tinel V50. During flood, the RDI Sentinel V50 estimates are higher than those from the Nortek
 364 Signature through the entire water column. During ebb, the estimates from the variance technique
 365 are biased low during the lower portion of the water column and they are higher during the second
 366 portion of it. During flood, the variance technique estimates remain lower for most of the water
 367 column. This difference highlights the importance of the tilt corrections incorporated in the new
 368 calculations of the Reynolds stresses as previously reported by Lu and Lueck (1999).

369 At Rich Passage the two methods are in good agreement, with slightly lower estimates from the
 370 variance technique through the water column. However, the average estimate from the TT ADV
 371 at this site is much higher, which might be explained by motion contamination at low frequencies
 372 in u'_{ch} (Kilcher et al. In revision).

373 *c. Vertical shear TKE Production*

374 The estimated Reynolds stresses together with the vertical shear are used to estimate the verti-
 375 cal shear TKE production rate. The uncertainty in the TKE production estimations is calculated
 376 following Williams and Simpson (2004) method, which is based in the variance of the product of
 377 two variables:

$$\sigma_{P_{ij}}^2 = \overline{u'_i u'_j}^2 \sigma_S^2 + \frac{\partial \overline{u_i}}{\partial x_j} \sigma_{RS}^2 + \sigma_S^2 \sigma_{RS}^2 \quad (14)$$

378 where $\sigma_{P_{ij}}$ is the uncertainty associated with the TKE production generated by the Reynolds stress
 379 $\overline{u'_i u'_j}$ and the shear $\frac{\partial \overline{u_i}}{\partial x_j}$. Then the uncertainty of the vertical shear production P (Eq. 6) is estimated
 380 as:

$$\sigma_P = \sqrt{\sigma_{P_{uchw}}^2 + \sigma_{P_{vchw}}^2 + \sigma_{P_{ww}}^2} \quad (15)$$

381 Figure 12 shows averaged vertical profiles of TKE production for both sites separated by ebb
 382 and flood tides and their respective uncertainty. In these plots, TKE production decreases with z ,

as expected for bottom-generated turbulence. The uncertainty in the TKE production increases with z , because $\sigma_{P_{\overline{w'w'}}$, which is the dominating term in the production uncertainty, increases with z . The $\sigma_{P_{\overline{w'w'}}$ uncertainty is dominated by its first term, $\overline{w'w'}\sigma_S^2$, which increases with z as would be expected as vertical fluctuations grow towards the mid water column, as the distance from the boundary increases. At Admiralty Inlet, TKE production uncertainties range from 2% closer to the bottom, up to 90% at the top of the measured profile during ebb (26% maximum uncertainty during flood). At Rich Passage, uncertainties range from 6% closer to the bottom, up to 90% at the top of the measured profile.

5. Application: Turbulent Kinetic Energy Balance

The analysis of the turbulent kinetic energy balance from field measurements usually assumes that TKE production balances TKE dissipation. The inclusion of the 5th beam in these new Acoustic Current Doppler Profilers allows for an improved estimation of TKE production; hence, a better closure of the TKE balance is possible. This improved TKE balance might indicate that other terms in the TKE balance, such as the TKE transport, are of importance, and it can be used to improve turbulence closure models in these environments.

Assuming that the buoyancy term is negligible at these well-mixed sites and that self-advection is small, the rate of change of TKE can be approximated as a local production-dissipation balance,

$$\frac{D}{Dt}(TKE) \approx P - \epsilon \quad (16)$$

Figure 11 shows the burst-averaged horizontal speed and vertical profiles in time of total TKE, TKE dissipation rate (from spectra), and TKE vertical production from the Nortek Signature data at both sites. At Admiralty Inlet, all three variables seem to be modulated by the stage of the tidal current, increasing as the velocity magnitude increases, however larger TKE, and TKE dissipation

404 and production rates are observed during ebb. A similar pattern is observed at Rich Passage,
405 where the variables are also modulated by the tidal currents, but larger values observed during the
406 stronger flood.

407 Figure 12 shows an approximate TKE budget as depth profiles of vertical shear TKE production
408 and TKE dissipation rates from the Nortek Signature data. Rates are averaged over all burst-
409 average horizontal speeds, for ebb and flood at each site. The expected balance is generally found,
410 however there are distinct patterns that likely are related to the lateral headland at Admiralty Inlet
411 and the vertical sill at Rich Passage.

412 During ebb at Admiralty Inlet, TKE production exceeds dissipation closer to the bottom and then
413 an approximate balance is observed above $z = 10.4$ m. During flood, production and dissipation
414 are approximately balance up to $z = 15.4$ m, and production exceeds dissipation in the higher
415 portion of the water column. At Rich Passage, production is balanced by dissipation for most
416 of the water column during ebb, except below $z = 5.4$ m, where dissipation exceeds production.
417 During flood, dissipation exceeds production through the entire profile.

418 Figure 13 shows scatter plots of TKE production versus TKE dissipation rates for all burst-
419 average velocities and all depths. The values are well correlated over several orders of magnitude,
420 albeit with significant scatter. At Admiralty Inlet, a near 1:1 balance between TKE production and
421 TKE dissipation during the most energetic conditions is observed. During less energetic condi-
422 tions, TKE production exceeds TKE dissipation, suggesting that the transport of turbulent kinetic
423 energy is of importance during such conditions. At Rich Passage, a near 1:1 balance between TKE
424 production and TKE dissipation is observed during all conditions.

6. Conclusions

Two new 5-beam acoustic current profilers, the Nortek Signature 1000 (KHz) AD2CP and the RDI Sentinel V50 are successfully used to measure turbulence at two energetic tidal channels: Admiralty Inlet and Rich Passage (Puget Sound, WA, U.S.A). Turbulent kinetic energy (TKE) production and dissipation rates are estimated from the measurements, and an approximate TKE budget is obtained.

The results illustrate the capabilities of 5-beam profilers for assessing high order turbulence parameters. The TKE frequency spectra from the Nortek Signature presents a low noise level, of $\mathcal{O}(10^{-4}) \text{ m}^2\text{s}^{-2}$, while the RDI Sentinel V50 presents a higher noise level of $\mathcal{O}(10^{-2}) \text{ m}^2\text{s}^{-2}$ that is comparable to the previous generation of profilers.

The lower noise observed on the Nortek Signature spectra might be attributed to its ability to sample faster (8 Hz when using all 5 beams), however when subsampling the Nortek Signature data to 2 Hz (the maximum possible with the RDI), the noise level in the TKE spectra remains of $\mathcal{O}(10^{-4}) \text{ m}^2\text{s}^{-2}$. The TKE spectra obtained with the Nortek Signature are in agreement with spectra from ADV measurements at both sites.

The lower noise level of the Nortek Signature enables observation of the inertial subrange of turbulence, and thus improved estimations of the TKE dissipation rate from both, TKE spectra and second order structure function of turbulence. TKE dissipation rates from the two methods agree well with each other through the water column, and also with estimates from ADV data.

Although the TKE spectra from the RDI Sentinel V50 does not allow the observation of the inertial subrange, the lower frequency portion of the spectra is well-resolved and in agreement with the estimates from the Nortek Signature and from the Nortek Vector. The RDI Sentinel V50 data can be used to estimate a synthetic vertical TKE spectra using the non-dimensional Kaimal

448 curves (Kaimal et al. 1972). These curves can be fit to the lower portion of the TKE spectra and
449 then used to extend the inertial subrange, and subsequently estimate the TKE dissipation rate.
450 However, the derivation of the Kaimal curves is based on a balance between TKE production and
451 dissipation, thus their application might only be appropriate at all depths where an approximate
452 Production - Dissipation balance is observed in the studied sites (Walter et al. 2011).

453 The use of all five beams enables the direct estimation of five out of six of the Reynolds stresses,
454 which allows for improved estimations of the TKE production rate and provides better information
455 for developing and validating turbulence closure models. The new Reynolds stresses calculations
456 include tilt corrections following the Dewey and Stringer (2007) method. At Admiralty Inlet,
457 Reynolds stresses estimates from the two profiling instruments are in agreement with estimates
458 from ADV at higher Reynolds stresses. The small differences may be attributed to instrument
459 separation and to remaining noise in the Reynolds stresses estimations.

460 The TKE dissipation rates and TKE production rates are used to analyze an approximate TKE
461 budget at Admiralty Inlet and at Rich Passage. In general, the expected balance is observed, how-
462 ever, distinct patterns are observed at the two sites, which are thought to be related to bathymetric
463 features that promote TKE advection and transport.

464 The most recent version of the Nortek Signature 1000 includes an integrated motion unit, which
465 enables instrument motion corrections, such that the instrument can also be mounted in buoys
466 and/or moorings. The new firmware version of the Nortek Signature supports High-Resolution
467 (HR) measurements, enabling high-sampling frequency measurements in velocity bins small as
468 0.02 m. The low Doppler noise of the Nortek Signature, similar to ADV noise levels, makes it
469 even suitable for lower turbulence environments. ADVs have been successfully used to estimate
470 TKE dissipation rates from TKE spectra in low turbulence environment such as lakes in Brand
471 et al. (2008) and in Vachon et al. (2010).

472 The turbulence parameters that can be obtained with these new instruments are useful for the
473 development and improvement of turbulence models, for the study of mixing processes, and for
474 predicting sediment transport. The methods presented in this paper are implemented in Matlab
475 and are available through the Matlab File Exchange website as 5-Beam Acoustic Doppler Current
476 Profiler Turbulence Methods: [http://www.mathworks.com/matlabcentral/fileexchange/](http://www.mathworks.com/matlabcentral/fileexchange/57551-mguerrap-5beam-turbulence-methods)
477 57551-mguerrap-5beam-turbulence-methods

478 *Acknowledgments.* We thank Joe Talbert and Alex de Klerk for deployment and recovery of the
479 instruments, and Andy Reay-Ellers for ship operations. We thank Levi Kilcher and Sam Harding
480 for motion-corrected ADV data (used for validation). Funding was provided by NAVFAC. Mari-
481 carmen Guerra thanks the Fulbright and the Becas-Chile Conicyt doctorate fellowship programs.

References

- Bassett, C., J. Thomson, and B. Polagye, 2013: Sediment-generated noise and bed stress in a tidal channel. *J. Geophys. Res. Oceans*, **118** (4), 2249–2265.
- Brand, A., D. McGinnis, B. Wehrli, and A. West, 2008: Intermittent oxygen flux from the interior into the bottom boundary of lakes as observed by eddy correlation. *Limnol. Oceanogr.*, **53** (5), 1997–2006.
- Brumley, B., R. Cabrera, K. Deines, and E. Terray, 1991: Performance of a broad-band acoustics Doppler current profiler. *J. Ocean. Eng.*, **16** (4).
- Dewey, R., and S. Stringer, 2007: Reynolds stresses and turbulent kinetic energy estimates from various adcp beam configurations: Theory. *Unpublished*, 1–35.
- Durgesh, V., J. Thomson, M. Richmond, and B. Polagye, 2014: Noise correction of turbulent spectra obtained from acoustic doppler velocimeters. *Flow Meas. Instrum.*, **37**, 29–41.
- Harding, S., L. Kilcher, and J. Thomson, In revision: Turbulence measurements from compliant moorings - part i: motion characterization. *J. Atmos. Oceanic Technol.*
- Kaimal, J., J. Wyngaard, Y. Izumi, and O. Coté, 1972: Spectral characteristics of surface-layer turbulence. *Q. J. R. Meteorol. Soc.*, **98** (417), 563–589.
- Kilcher, L., S. Harding, J. Thomson, and S. Nylund, In revision: Turbulence measurements from compliant moorings - part i: motion correction. *J. Atmos. Oceanic Technol.*
- Kolmogorov, A., 1941: Dissipation of energy in the locally isotropic turbulence. *Dokl. Akad. Nauk SSR*, **30**, 301–305.

Lu, Y., and R. Lueck, 1999: Using a broadband adcp in a tidal channel. part ii: Turbulence. *J. Atmos. Oceanic Technol.*, **16** (11), 1568–1579.

Lumley, J., and E. Terray, 1983: Kinematics of turbulence convected by a random wave field. *J. Phys. Oceanogr.*, **13**, 2000–2007.

McCaffrey, K., B. Fox-Kemper, P. Hamlington, and J. Thomson, 2015: Characterization of turbulence anisotropy, coherence, and intermittency at a prospective tidal energy site: Observational data analysis. *Renewable Energy*, **76**, 441–453.

McMillan, J., and A. Hay, 2017: Spectral and structure function estimates of turbulence dissipation rates in a high-flow tidal channel using broadband adcps. *J. Atmos. Oceanic Technol.*, **34** (1), 5–20.

McMillan, J., A. Hay, R. Lueck, and F. Wolk, 2016: Rates of dissipation of turbulent kinetic energy in a high reynolds number tidal channel. *J. Atmos. Oceanic Technol.*, **33** (4), 817–837.

Pope, S., 2001: *Turbulent flows*. IOP Publishing.

Richard, J., J. Thomson, B. Polagye, and J. Bard, 2013: Method for identification of doppler noise levels in turbulent flow measurements dedicated to tidal energy. *Int. J. Marine Energy*, **3**, 52–64.

Rippeth, T., J. Simpson, E. Williams, and M. Inall, 2003: Measurement of the rates of production and dissipation of turbulent kinetic energy in an energetic tidal flow: Red wharf bay revisited. *J. Phys. Oceanogr.*, **33** (9), 1889–1901.

Rusello, P., and E. Cowen, 2011: Turbulent dissipation estimates from pulse coherent doppler instruments. *Proc. IEEE/OES 10th Current, Waves and Turbulence Measurements (CWTM)*, Monterey, CA., IEEE, 167–172.

- 523 Sreenivasan, K., 1995: On the universality of the kolmogorov constant. *Phys. Fluids*, **7** (11),
524 2778–2784.
- 525 Stacey, M., S. Monismith, and J. Burau, 1999: Measurements of reynolds stress profiles in un-
526 stratified tidal flow. *J. Geophys. Res.*, **104**, 10 935–10 949.
- 527 Thomson, J., 2012: Wave breaking dissipation observed with swift drifters. *J. Atmos. Oceanic*
528 *Technol*, **29** (12), 1866–1882.
- 529 Thomson, J., L. Kilcher, M. Richmond, J. Talbert, A. deKlerk, B. Polagye, M. Guerra, and R. Cien-
530 fuegos, 2013: Tidal turbulence spectra from a compliant mooring. *Proc. of the 1st Marine En-*
531 *ergy Technical Symposium (METS), Washington D.C.*
- 532 Thomson, J., B. Polagye, V. Durgesh, and M. Richmond, 2012: Measurements of turbulence at
533 two tidal energy sites in Puget Sound, WA. *IEEE J. Oceanic Eng.*, **37** (3), 363–374.
- 534 Vachon, D., Y. Prairie, and J. Cole, 2010: The relationship between near-surface turbulence and
535 gas transfer velocity in freshwater systems and its implications for floating chamber measure-
536 ments of gas exchange. *Limnol. Oceanogr.*, **55** (4), 1723–1732.
- 537 Walter, R., N. Nidzieko, and S. Monismith, 2011: Similarity scaling of turbulence spectra and
538 cospectra in a shallow tidal flow. *J. Geophys. Res. Oceans*, **116** (C10).
- 539 Wiles, P., T. Rippeth, H. J. Simpson, and P. Hendricks, 2006: A novel technique for measuring the
540 rate of turbulent dissipation in the marine environment. *Geophys. Res. Lett.*, **33** (21).
- 541 Williams, E., and J. Simpson, 2004: Uncertainties in estimates of reynolds stress and the produc-
542 tion rate using the adcp variance method. *J. Atmos. Ocean. Technol*, **21** (2), 347–357.

543 **LIST OF TABLES**

544 **Table 1.** Summary of deployments and sampling parameters at Admiralty Inlet and Rich
545 Passage. 29

TABLE 1. Summary of deployments and sampling parameters at Admiralty Inlet and Rich Passage.

Location	Admiralty Inlet	Admiralty Inlet	Admiralty Inlet	Rich Passage	Rich Passage
Instrument	Nortek Signature 1000	RDI Sentinel V50	Nortek Vector ADV	Nortek Signature 1000	Nortek Vector ADV
Latitude (°)	48.1522	48.1517	48.1524	47.5887	47.5887
Longitude (°)	-122.6852	-122.6858	-122.6868	-122.5641	-122.5641
Water Depth (m)	50	50	50	24	24
Deployment Duration (days)	2	2	2	2	0.1
Sampling Frequency (Hz)	8	2	16	8	16
Burst-Average (min)	10	10	10	10	10
Δz (m)	1	1	-	1	-
Distance to first cell (m)	0.5	0.5	-	0.5	-
Range (m)	20.5	20.5	-	15.5	-
z target (m)	-	-	10	-	17
Single ping error (ms^{-1})	0.016	0.003	0.02	0.016	0.02
Empirical error (ms^{-1})	0.027	0.054	0.011	0.027	0.011
Pitch °	2.26 ± 0.005	4.45 ± 0.06	-	0.35 ± 0.002	-
Roll °	0.36 ± 0.02	-1.61 ± 0.01	-	-1.19 ± 0.004	-

LIST OF FIGURES

Fig. 1.	Bathymetry and location of the two tidal channels: a) Puget Sound in Washington, U.S.A., b) Admiralty Inlet (AI) and c) Rich Passage (RP). Red dots indicate instruments location.	32
Fig. 2.	Vertical profiles and time series of along-channel velocities measured with the Nortek Signature: a), b) at Admiralty Inlet, and c), d) at Rich Passage. In a) and c) black dashed line indicates depth corresponding to the time series (as $z = 10.4$ m from sea-bottom). In b) and d), grey dots correspond to measured along-channel velocity, and black line corresponds to 10 minute burst-averaged along-channel velocity. Burst-averaged along-channel velocity measured with the TTM ADV at Admiralty Inlet is included as a black dashed line in b).	33
Fig. 3.	TKE spectra at $z = 10.4$ m for different mean flows (by color): a), b) at Admiralty Inlet, and c), d) at Rich Passage. Dashed black line is proportional to $f^{-5/3}$. Inset plots show burst-average horizontal speed vertical profiles (also by color); dot-dashed line shows $z = 10.4$ m in the profiles. In the Admiralty Inlet plots, spectra from the RDI Sentinel V50 data are included as grey curves, and the range of spectra from the TTM ADV data is included as a light pink are. Dashed line corresponds to averaged spectra from ADV data.	34
Fig. 4.	TKE spectra at maximum ebb and flood mean flow conditions at different depths (by color): a), b) at Admiralty Inlet, and c), d) at Rich Passage. Dashed black line is proportional to $f^{-5/3}$. Inset plots show corresponding mean flow vertical profile.	35
Fig. 5.	Spatial structure function at $z = 10.4$ m for different mean flows (by color): a), b) at Admiralty Inlet, and c), d) at Rich Passage. The dashed line is proportional to $r^{2/3}$. Inset plots show mean flow vertical profiles (also by color); the dot-dashed line corresponds to $z = 10.4$ m. In the Admiralty Inlet plots, structure functions from the RDI Sentinel V50 data are included as grey curves.	36
Fig. 6.	Average vertical profiles of TKE dissipation rate at: a), b) at Admiralty Inlet, and c), d) at Rich Passage. In blue from the TKE spectra and in black from the turbulence structure function. Blue dots correspond to TKE dissipation rate estimates from the TTM ADV spectra.	37
Fig. 7.	Vertical shear Reynolds stress $\overline{(u'_{ch}w')}$ at Admiralty Inlet: from TTM ADV data (x-axis), and from Nortek Signature and RDI Sentinel V50 estimated using Dewey and Stringer (2007) 5-beam method (y-axis). Blue and red dots are averages binned by $\overline{u'_{ch}w'}$ from the TTM ADV measurements. Black-dashed line correspond to $y = x$. Averaged data correlation coefficients: 0.6 (Nortek Signature to TTM ADV), 0.05 (RDI Sentinel V50 to TTM ADV).	38
Fig. 8.	Horizontal burst-averaged speed and vertical profiles of Reynolds stresses in time estimated using Dewey and Stringer (2007) 5-beam method at Admiralty Inlet: a) Mean flow, b) $\overline{u'^2_{ch}}$, c) $\overline{v'^2_{ch}}$, d) $\overline{w'^2}$, e) $\overline{u'_{ch}w'}$, and f) $\overline{v'_{ch}w'}$. Slack conditions are marked in grey.	39
Fig. 9.	Horizontal burst-averaged speed and vertical profiles of Reynolds stresses in time estimated using Dewey and Stringer (2007) 5-beam method at Rich Passage: a) Mean flow, b) $\overline{u'^2_{ch}}$, c) $\overline{v'^2_{ch}}$, d) $\overline{w'^2}$, e) $\overline{u'_{ch}w'}$, and f) $\overline{v'_{ch}w'}$. Slack conditions are marked in grey.	40
Fig. 10.	Average vertical shear Reynolds stress $\overline{(u'_{ch}w')}$ profiles estimated using Dewey and Stringer (2007) 5-beam method at: a), b) at Admiralty Inlet, and c), d) at Rich Passage. In blue from the Nortek Signature data, in red from the RDI Sentinel V50 data. Dashed lines correspond	

587	to estimates using the original variance technique with no tilt corrections (Stacey et al. 1999).	
588	Blue dots correspond to estimates from the ADV data.	41
589	Fig. 11. Vertical profiles of TKE dissipation and production rates in time at Admiralty Inlet (left) and	
590	at Rich Passage (right). Panels show: a) and e) Mean horizontal speed, b) and f) Total TKE,	
591	c) and g) TKE dissipation rate, d) and h) TKE production rate.	42
592	Fig. 12. An approximate TKE budget shown using average TKE dissipation rates from the two meth-	
593	ods and TKE shear production from Reynolds stresses from the Nortek Signature data: a),	
594	b) at Admiralty Inlet, and c), d) at Rich Passage.	43
595	Fig. 13. TKE Dissipation Rate and TKE Production for all \bar{u} and all depths: a), b) at Admiralty Inlet	
596	and b), c) at Rich Passage. Black dots represent mean values of dissipation and production	
597	binned by dissipation. Red dashed line corresponds to $y = x$. In the plots showing the TKE	
598	dissipation rate from the structure function, the dashed grey line represents the limit of TKE	
599	dissipation detection when using the turbulence structure function.	44

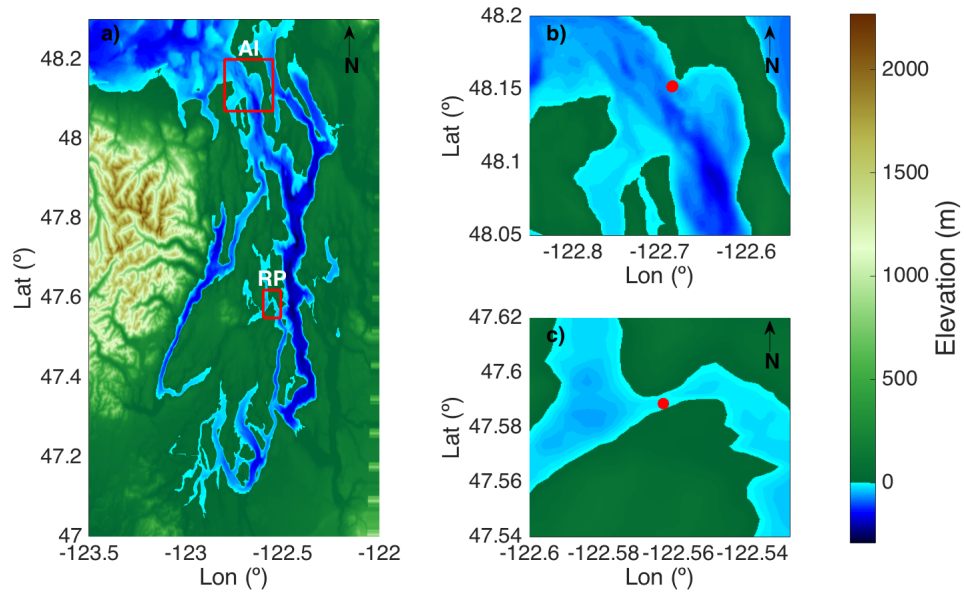


FIG. 1. Bathymetry and location of the two tidal channels: a) Puget Sound in Washington, U.S.A., b) Admiralty Inlet (AI) and c) Rich Passage (RP). Red dots indicate instruments location.

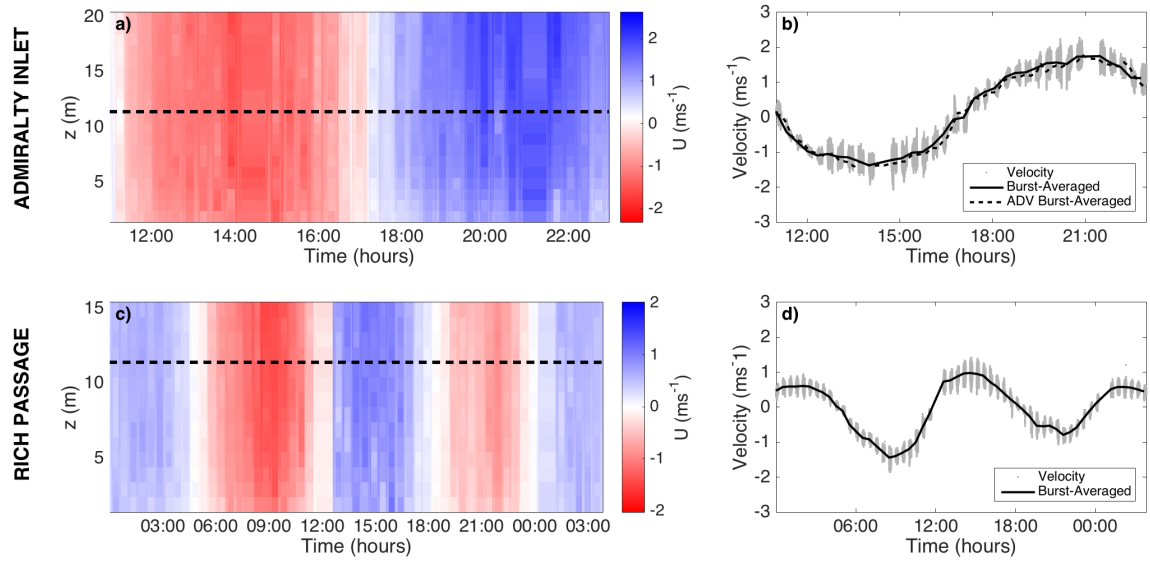


FIG. 2. Vertical profiles and time series of along-channel velocities measured with the Nortek Signature: a),
 b) at Admiralty Inlet, and c), d) at Rich Passage. In a) and c) black dashed line indicates depth corresponding to
 the time series (as $z = 10.4$ m from sea-bottom). In b) and d), grey dots correspond to measured along-channel
 velocity, and black line corresponds to 10 minute burst-averaged along-channel velocity. Burst-averaged along-
 channel velocity measured with the TTM ADV at Admiralty Inlet is included as a black dashed line in b).

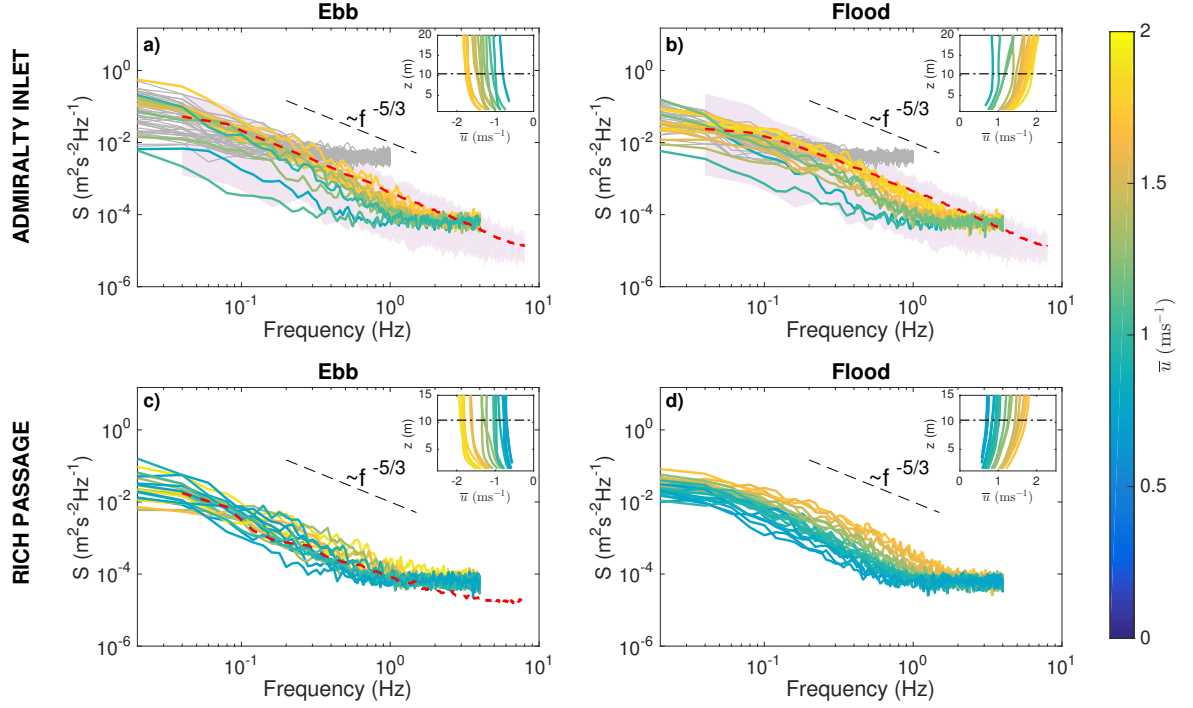


FIG. 3. TKE spectra at $z = 10.4$ m for different mean flows (by color): a), b) at Admiralty Inlet, and c), d) at Rich Passage. Dashed black line is proportional to $f^{-5/3}$. Inset plots show burst-average horizontal speed vertical profiles (also by color); dot-dashed line shows $z = 10.4$ m in the profiles. In the Admiralty Inlet plots, spectra from the RDI Sentinel V50 data are included as grey curves, and the range of spectra from the TTM ADV data is included as a light pink are. Dashed line corresponds to averaged spectra from ADV data.

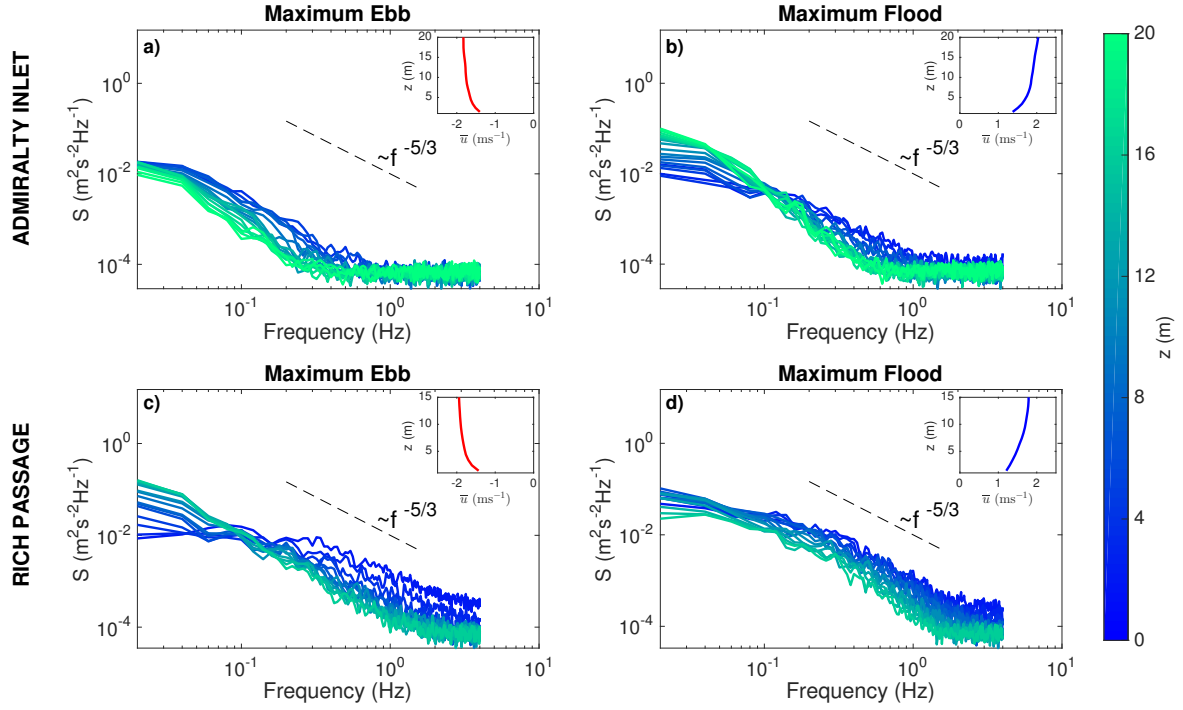
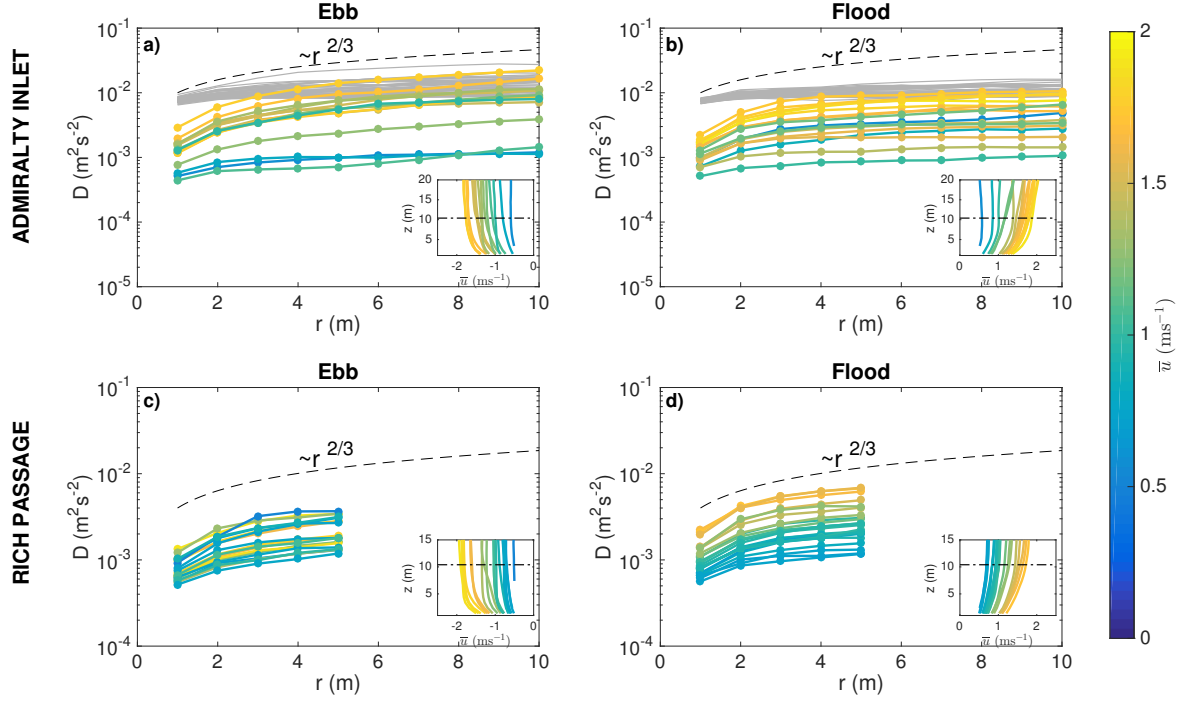


FIG. 4. TKE spectra at maximum ebb and flood mean flow conditions at different depths (by color): a), b) at Admiralty Inlet, and c), d) at Rich Passage. Dashed black line is proportional to $f^{-5/3}$. Inset plots show corresponding mean flow vertical profile.



615 FIG. 5. Spatial structure function at $z = 10.4$ m for different mean flows (by color): a), b) at Admiralty Inlet,
 616 and c), d) at Rich Passage. The dashed line is proportional to $r^{2/3}$. Inset plots show mean flow vertical profiles
 617 (also by color); the dot-dashed line corresponds to $z = 10.4$ m. In the Admiralty Inlet plots, structure functions
 618 from the RDI Sentinel V50 data are included as grey curves.

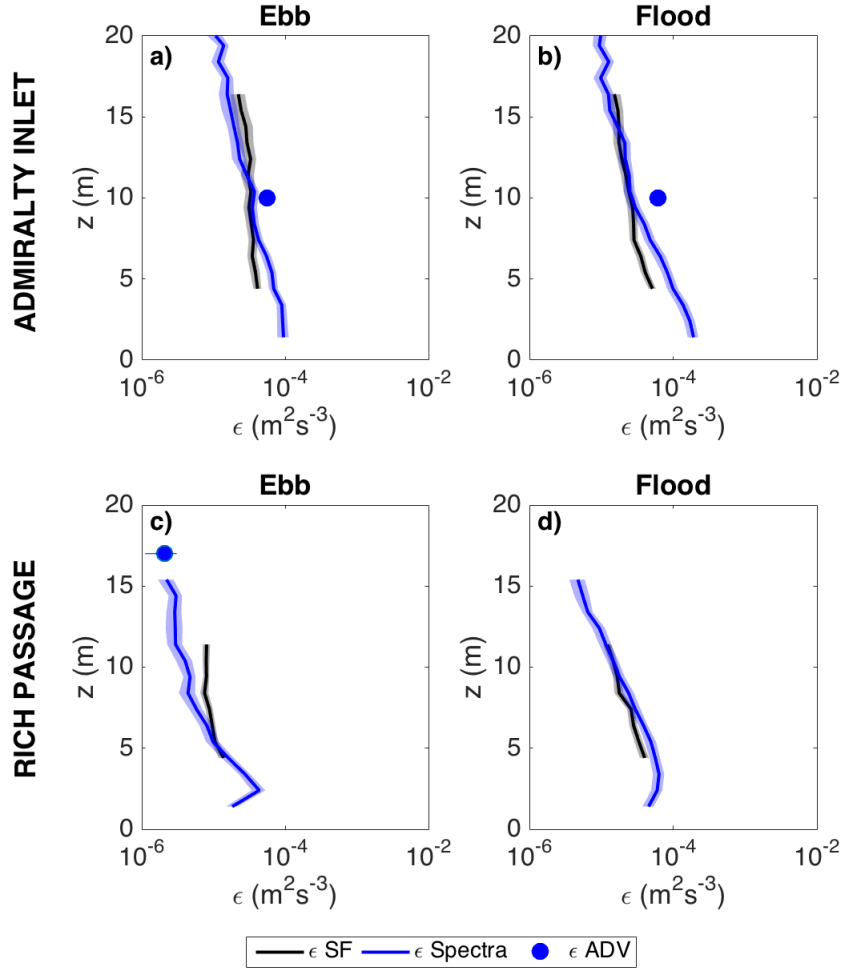


FIG. 6. Average vertical profiles of TKE dissipation rate at: a), b) at Admiralty Inlet, and c), d) at Rich Passage. In blue from the TKE spectra and in black from the turbulence structure function. Blue dots correspond to TKE dissipation rate estimates from the TTM ADV spectra.

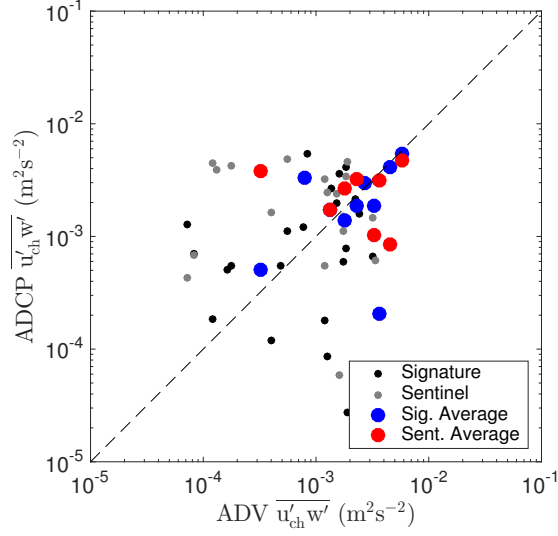


FIG. 7. Vertical shear Reynolds stress $\overline{u'_{ch} w'}$ at Admiralty Inlet: from TTM ADV data (x-axis), and from Nortek Signature and RDI Sentinel V50 estimated using Dewey and Stringer (2007) 5-beam method (y-axis). Blue and red dots are averages binned by $\overline{u'_{ch} w'}$ from the TTM ADV measurements. Black-dashed line correspond to $y = x$. Averaged data correlation coefficients: 0.6 (Nortek Signature to TTM ADV), 0.05 (RDI Sentinel V50 to TTM ADV).

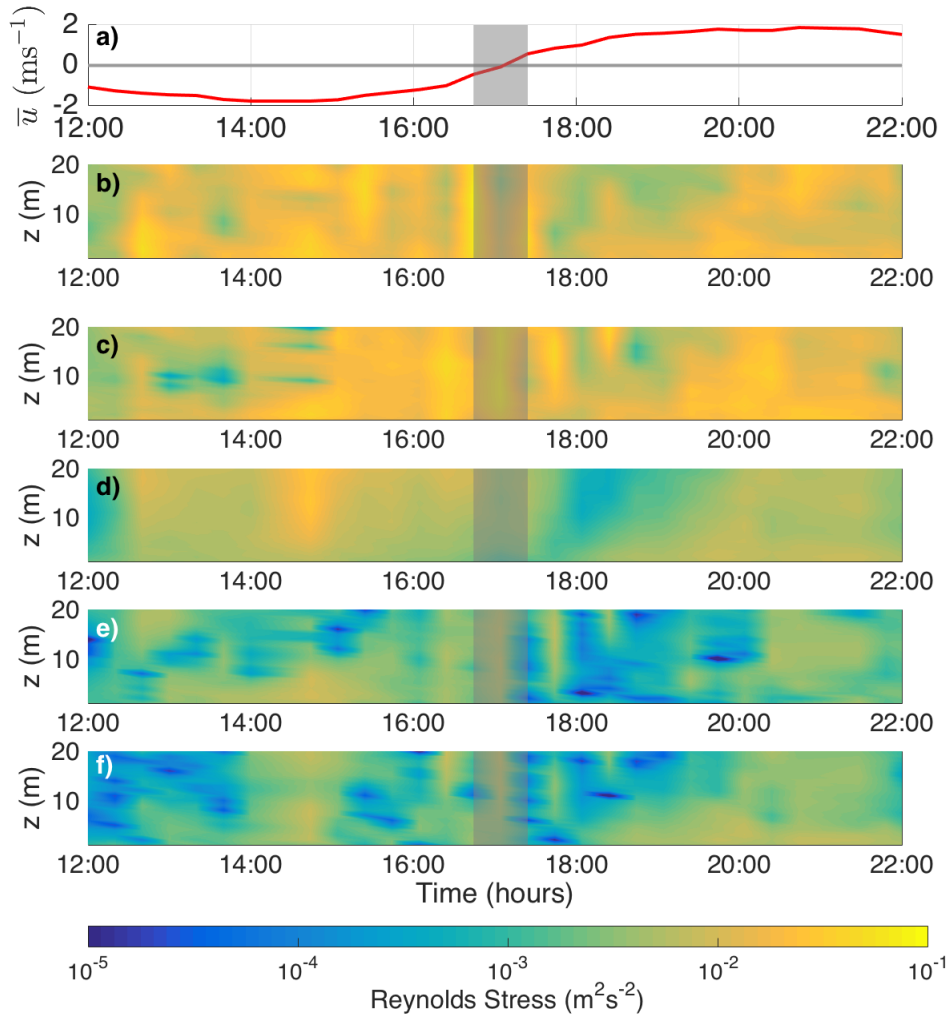


FIG. 8. Horizontal burst-averaged speed and vertical profiles of Reynolds stresses in time estimated using Dewey and Stringer (2007) 5-beam method at Admiralty Inlet: a) Mean flow, b) $\overline{u_{ch}^2}$, c) $\overline{v_{ch}^2}$, d) $\overline{w^2}$, e) $\overline{u'_{ch} w'}$, and f) $\overline{v'_{ch} w'}$. Slack conditions are marked in grey.

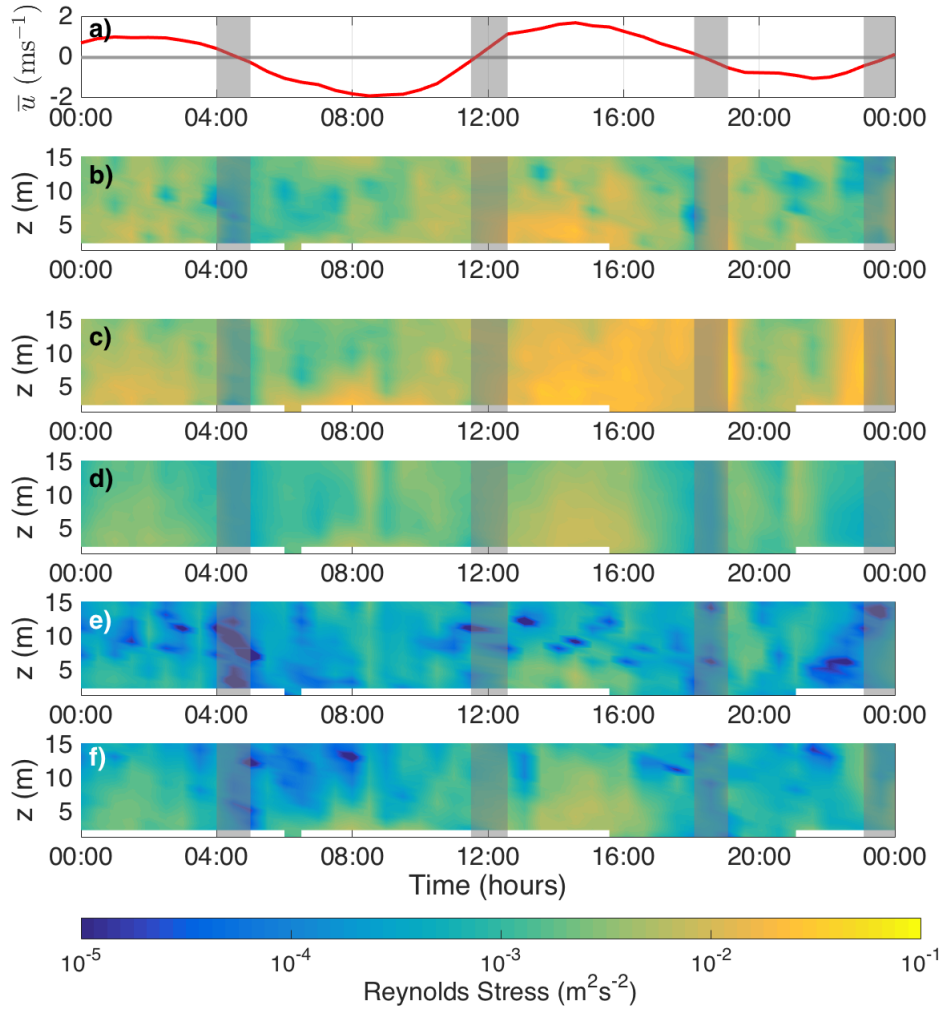


FIG. 9. Horizontal burst-averaged speed and vertical profiles of Reynolds stresses in time estimated using Dewey and Stringer (2007) 5-beam method at Rich Passage: a) Mean flow, b) $\overline{u'^2_{ch}}$, c) $\overline{v'^2_{ch}}$, d) $\overline{w'^2}$, e) $\overline{u'_{ch}w'}$, and f) $\overline{v'_{ch}w'}$. Slack conditions are marked in grey.

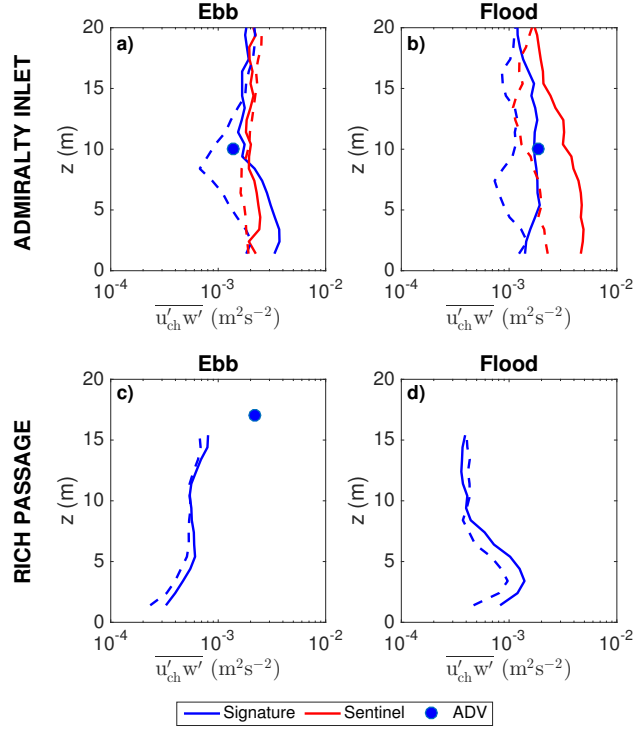


FIG. 10. Average vertical shear Reynolds stress ($\overline{u'_{ch} w'}$) profiles estimated using Dewey and Stringer (2007) 5-beam method at: a), b) at Admiralty Inlet, and c), d) at Rich Passage. In blue from the Nortek Signature data, in red from the RDI Sentinel V50 data. Dashed lines correspond to estimates using the original variance technique with no tilt corrections (Stacey et al. 1999). Blue dots correspond to estimates from the ADV data.

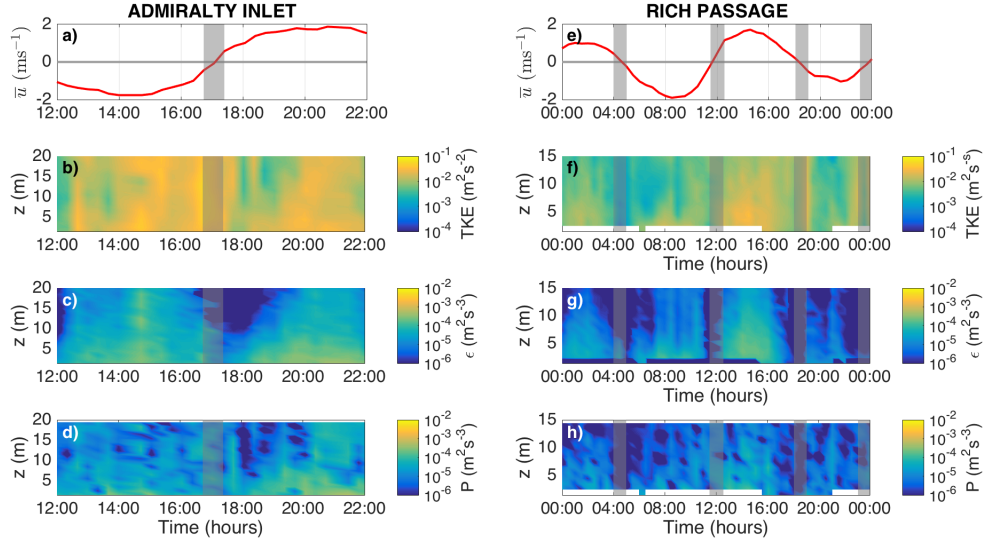


FIG. 11. Vertical profiles of TKE dissipation and production rates in time at Admiralty Inlet (left) and at Rich Passage (right). Panels show: a) and e) Mean horizontal speed, b) and f) Total TKE, c) and g) TKE dissipation rate, d) and h) TKE production rate.

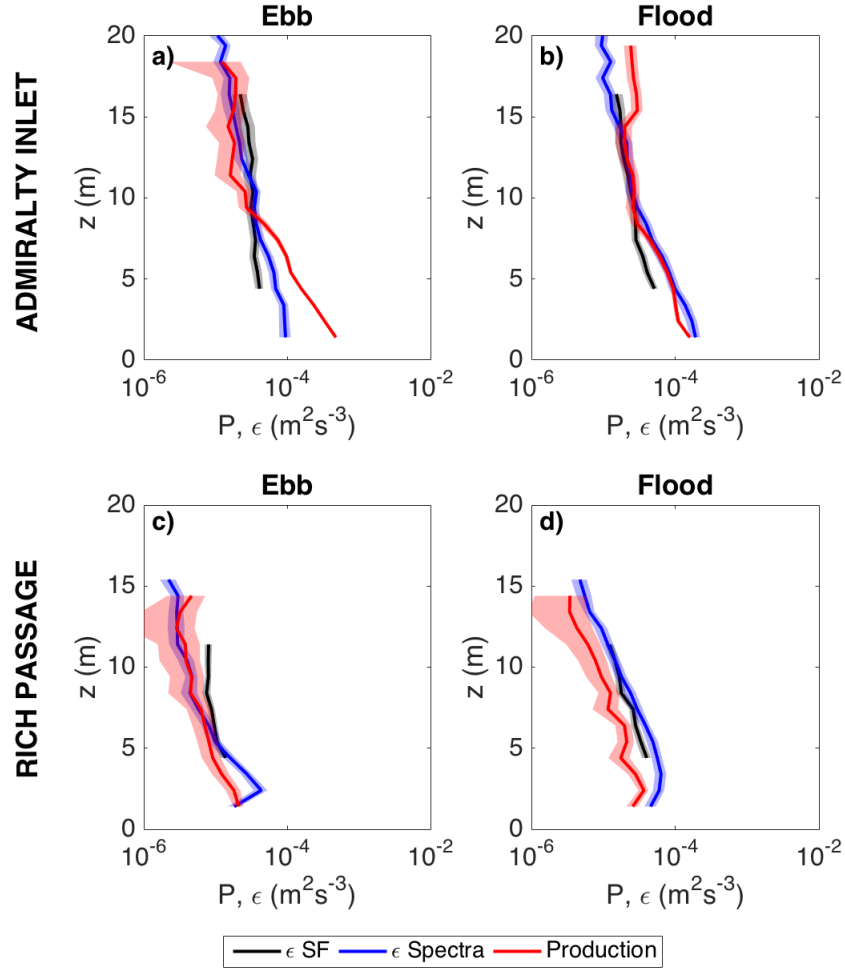


FIG. 12. An approximate TKE budget shown using average TKE dissipation rates from the two methods and TKE shear production from Reynolds stresses from the Nortek Signature data: a), b) at Admiralty Inlet, and c), d) at Rich Passage.

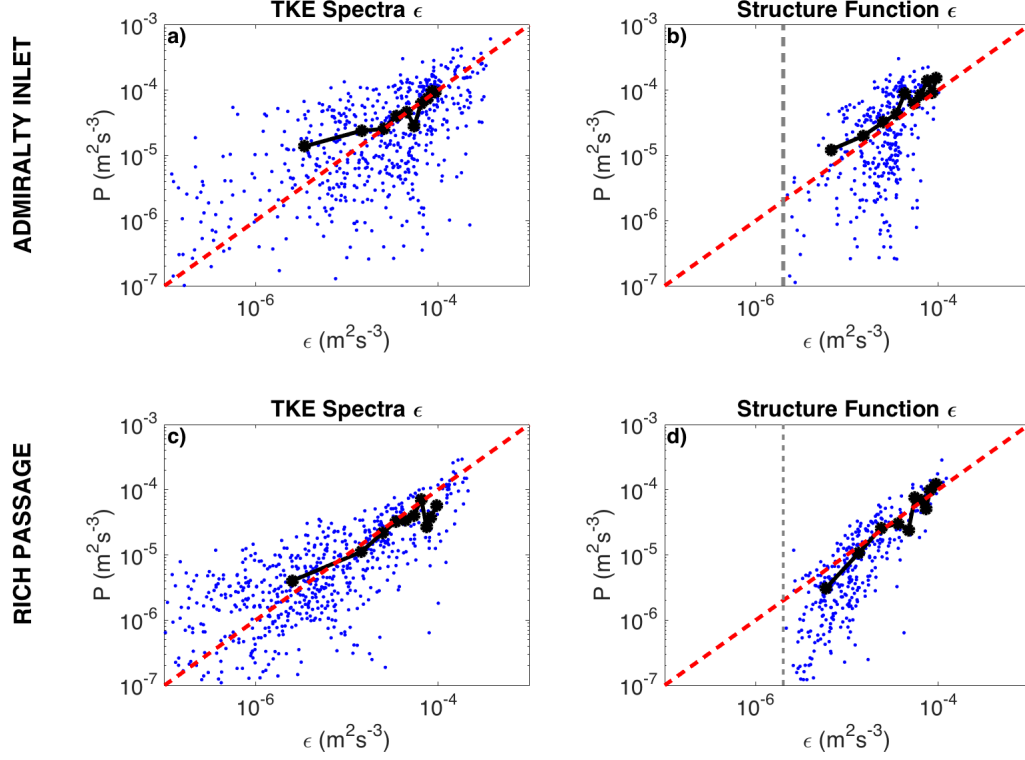


FIG. 13. TKE Dissipation Rate and TKE Production for all \bar{u} and all depths: a), b) at Admiralty Inlet and b),
c) at Rich Passage. Black dots represent mean values of dissipation and production binned by dissipation. Red
dashed line corresponds to $y = x$. In the plots showing the TKE dissipation rate from the structure function, the
dashed grey line represents the limit of TKE dissipation detection when using the turbulence structure function.